Experimental Investigation of an Integrated Flow-Cytometry Chip for White Blood Cell Focusing.

Author

HUDAIR SAMAD

00000118349

Supervisor

Dr. Emad Uddin

DEPARTMENT OF DESIGN & MANUFACTURING ENGINEERING

SCHOOL OF MECHANICAL & MANUFACTURING ENGINEERING (SMME)

NATIONAL UNIVERSITY OF SCIENCES AND TECHNOLOGY

H-12, ISLAMABAD

Experimental Investigation of an Integrated Flow-Cytometry Chip for White Blood cell Focusing.

HUDAIR SAMAD

00000118349

In partial fulfillment of the requirements for the degree of

MS Design and Manufacturing Engineering

Thesis Supervisor:

Dr. Emad Uddin

Thesis Supervisor's Signature: _____

Department of Design & Manufacturing Engineering

School of Mechanical & Manufacturing Engineering (SMME)

National University Of Sciences and Technology

H-12, Islamabad

National University of Sciences & Technology

MASTER THESIS WORK

We hereby recommend that the dissertation prepared under our supervision by: Hudair Samad, Reg # 00000118349 Titled: "*Experimental Investigation of an Integrated Flow-Cytometry Chip for White Blood cell Focusing"* be accepted in partial fulfillment of the requirements for the award of Masters of Science in Design and Manufacturing Engineering Degree with (grade)

Examination Committee Members

1. Name: Dr. Muhammad Sajid Signature: _____

2. Name: Dr. Sami Ur Rahman Shah Signature: _____

3. Name: Dr. Aamir Mubashir Signature: _____

Supervisor's name: Dr. Emad Uddin Signature: _____
Date: __/__/2017

_____ _____
Head of Department Date

COUNTERSINGED

_____
Dean/Principal

Date: _____

DECLARATION

I certify that this research work titled "*Experimental Investigation of an Integrated Flow-Cytometry Chip for White Blood cell Focusing."* is my own work. The work has not been presented elsewhere for assessment. The material that has been used from other sources it has been properly acknowledged / referred.

Hudair Samad
00000118349

CERTIFICATE FOR PLAGIARISM

It is certified that PhD/M.Phil/MS Thesis Titled ***Experimental Investigation of an Integrated Flow-Cytometry Chip for White Blood cell*** **Focusing** by **Hudair Samad** has been examined by us. We undertake the follows:

a. Thesis has significant new work/knowledge as compared already published or are under consideration to be published elsewhere. No sentence, equation, diagram, table, paragraph or section has been copied verbatim from previous work unless it is placed under quotation marks and duly referenced.
b. The work presented is original and own work of the author (i.e. there is no plagiarism). No ideas, processes, results or words of others have been presented as Author own work.
c. There is no fabrication of data or results which have been compiled/analyzed.
d. There is no falsification by manipulating research materials, equipment or processes, or changing or omitting data or results such that the research is not accurately represented in the research record.
e. The thesis has been checked using TURNITIN (copy of originality report attached) and found within limits as per HEC plagiarism Policy and instructions issued from time to time.

Name & Signature of Supervisor

_____

Signature**:**_____

COPYRIGHT STATEMENT

Dedicated to My Father

Without Whom I am Nothing

ACKNOWLEDGEMENTS

In the name of Allah, the Magnificent, the Merciful.

Research work is a never ending struggle, and I am happy to have support from family and friends. I have my fair share of mistakes along the way, but as Einstein once said, “Anyone who has never made a mistake has never tried anything new.” After each road block, Dr. Emad has been a beacon of hope, enlightening the path; guiding. I am forever in gratitude to Dr. Emad Uddin, my research supervisor also the encouragement and guidance of my Guidance and Examination Committee is estimable.

I would also want to pay my regard to the management of “Smart PCB’s” and specially Mr.Imran-ullah and the management of “Lahore University of Management Sciences” for their support in the manufacturing process.

I am profusely thankful to my parents and siblings who have continuous support for me throughout in every department of my life. I also owe my deep graditude to my fellows, Yasir Abassi, Abdul Baseer, Ch.Abdullah, Husnain ul Abiden, Mujahid Saeed and M.Usman as their construstive criticism and support helped me a lot during this journy.

Last but not least I feel lucky to have the support of Miss Rabia Zahoor for “Agricultural University Faisalabad” as she was there for me in every hard time to support me morally and technically.

To everyone, who were a part of this journey with me, thank you and wish you all the best in future.

ABSTRACT

The interaction of the vortex and the flexible flag in wake of a bluff body is a common occurrence in nature and in engineering fields. The limited availability and the environmental impact of fossil fuels motivate the development of renewable energy sources. Considerable efforts are focused on use of renewable energy from natural resources such as flowing water, rain, tides, wind, sunlight, geothermal heat and biomass. Renewable energy from small-scale hydro, modern biomass, wind, solar, geothermal and biofuels accounted for global energy consumption was 2.7% in 2008, increased to 5.8% in 2012 and is growing very rapidly.

Aquatic animals utilize oscillatory motions of the fins or wings to achieve propulsion and maneuvering. They extract energy from the incoming vortices or unsteady flows. Zhu et al. showed that the caudal fin of a fish can absorb energy from vortices shed from the dorsal fins to increase the propulsion efficiency. Also dead fish is capable of moving upstream within the Karman vortex street generated by a D-shape cylinder. Bio-inspired energy harvesting devices based on the oscillatory motions of foils had been developed by using an oscillating wing to extract energy from the unsteady flow fields generated by the free-surface waves. The application of flapping wings to extract energy from uniform flows was first proposed by McKinney and De Laurier. Both experiments and theoretical analyses discovered that a foil submerged in the free surface could propel by using the energy from the incoming waves. With the growing importance of renewable energy, the interest in this novel concept has been rekindled in the past few years. Allen and Smits examined the response of the piezoelectric membrane to vortex shedding Introduction.

Table of Contents

List of Figures

Chapter: 1

INTRODUCTION

The interaction of the vortex and the flexible flag in wake of a bluff body is a common occurrence in nature and in engineering fields. The limited availability and the environmental impact of fossil fuels motivate the development of renewable energy sources. Considerable efforts are focused on use of renewable energy from natural resources such as flowing water, rain, tides, wind, sunlight, geothermal heat and biomass. Renewable energy from small-scale hydro, modern biomass, wind, solar, geothermal and biofuels accounted for global energy consumption was 2.7% in 2008, increased to 5.8% in 2012 and is growing very rapidly [1].

From a hydrodynamic point of view, experimental evidence has supported the assertion that the appropriate synchronization of the positioning in of flag in the wake of the bluff body can be advantageous by increasing the hydrodynamic resistance due to wake interactions and introducing significant energy harvesting[2-6]. Nevertheless, the phenomenon of the hydrodynamic interactions of a flag in the wake of a bluff body has not yet well understood, and a more detailed understanding of the mechanisms would be desirable.

Aquatic animals utilize oscillatory motions of the fins or wings to achieve propulsion and maneuvering [7]. They extract energy from the incoming vortices or unsteady flows. Zhu et al. [8] showed that the caudal fin of a fish can absorb energy from vortices shed from the dorsal fins to increase the propulsion efficiency. Also dead fish

is capable of moving upstream within the Karman vortex street generated by a D-shape cylinder [9]. Bio-inspired energy harvesting devices based on the oscillatory motions of foils had been developed by using an oscillating wing to extract energy from the unsteady flow fields generated by the free-surface waves. The application of flapping wings to extract energy from uniform flows was first proposed by McKinney and De Laurier [10]. Both experiments and theoretical analyses discovered that a foil submerged in the free surface could propel by using the energy from the incoming waves [11-14]. With the growing importance of renewable energy, the interest in this novel concept has been rekindled in the past few years. Allen and Smits [2] examined the response of the piezoelectric membrane to vortex shedding

The current study provides the dynamics of flow around a flexible flag (eel) in the wake of a D-shaped half cylinder subjected to a two-dimensional uniform viscous flow. The flexible flag is subjected to passive flapping by the combination of heaving and pitching oscillations. The introduction of an actively flapping flexible flag in the downstream of a D-shaped half cylinder imparts more complicated interaction phenomenon. There are some analytical and numerical studies on the energy harvesting eel but the detail investigation and optimization of the parameters is the missing link [15]. This study provides necessary insights towards better understanding of the dynamics of flapping flexible flag in the wake of the D-shaped half cylinder subjected to viscous flow and the optimization of the parameters for energy harvesting eel for passive mode of flapping. The dependence of the bending energy on the stream wise gap distance between the D-shaped half cylinder and the downstream flag, the length and the bending rigidity of the downstream flag, effect of the bending energy on the actively flapping downstream flexible flag for the variable pitching and heaving phase difference, and the pitching and heaving amplitude were examined in

detail. This study provides the intriguing results: within a range of the flapping conditions, the flapping downstream flag can experience a distinct drag enhancement thus producing more energy. Moreover, the vortices shed by the D-shaped half cylinder interacts with the downstream flag via two modes of interaction for passive flapping i:e; constructive and destructive mode , which explains the significant drag changes experienced by the flexible structures In the next section the formulation of the problem, numerical method and Experimental method is briefly described. In Section 3, the results and discussion are presented. Finally, conclusions are drawn in Section 4.

Chapter: 2

METHODOLOGY.

In simulation, the dynamics of energy harvesting flexible flag behind a half cylinder undergoing passive flapping mode subjected to a uniform viscous flow by using the immersed boundary method. The analysis was carried out under different conditions by varying S/D, L/D and γ. While in Experimentation Piezo Electric material is used as energy harvesting Flag, Teflon cylinders of three different diameter is used as bluff body.12volt Dc fan with streamline Grill is used as Variable Velocity Air source. Steel Fixture is used for experimental setup. Two LED lights (YN300II) of 2000 lumens is used to illuminate the flag motion. High Frame Rate Camera (Sony RX100 IV) is used to Capture the motion of Energy Harvesting Flag at 1000 frames per second.

Numerical methodology

A flexible flag in the wake of a D-shaped half cylinder was subjected to the two-dimensional viscous flow. A schematic diagram of the geometric configuration and the coordinate system is shown in figure 1.

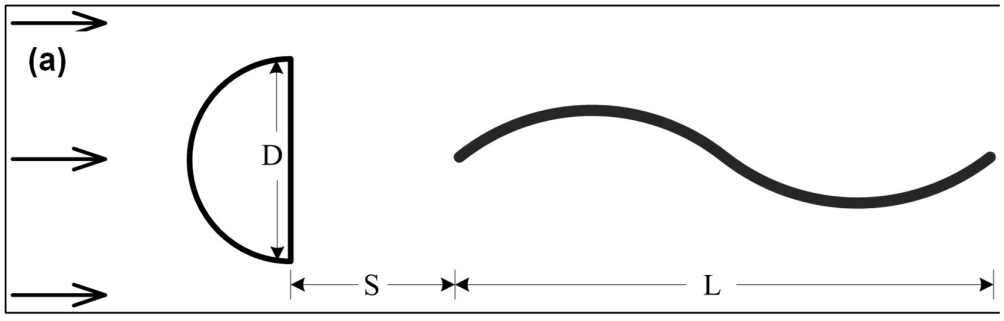

Figure 1: Figure 1(a) Schematic, (b)Wind tunnel, (c) Test section, (d) Voltage measurement

The distance between the D-shaped half cylinder and the flexible flag was varied by adjusting the stream-wise gap distance "S". The head of the downstream flag was fixed under a simply supported boundary condition and the boundary condition for the free end was considered at the tails. The rigid D-shaped half cylinder is placed at the center (0,0) with diameter "D". The fluid domain was defined by an Eulerian coordinate system, and a separate Lagrangian coordinate system was applied to the flexible flag. The flexible flag in a viscous flow were modeled using an improved immersed boundary method (Huang *et al.* [31]), in which the governing equations of the fluid flow and the flexible flag was solved in each coordinate system, and the interactions among components was calculated using a feedback law.

The fluid motion was governed by the incompressible Navier-Stokes and continuity equations,

$$\frac{\partial \boldsymbol{u}}{\partial t} + \boldsymbol{u} \cdot \nabla \boldsymbol{u} = -\nabla p + \frac{1}{\mathrm{Re}} \nabla^2 \boldsymbol{u} + \boldsymbol{f} \,, \tag{1}$$

$$\nabla \cdot \boldsymbol{u} = 0, \tag{2}$$

where $\boldsymbol{u}$ is the velocity vector, p is the pressure, $\boldsymbol{f}$ is the momentum force applied to enforce the no-slip conditions along the immersed boundary, and the Reynolds number Re is defined by $\mathrm{Re} = \rho_0 U_\infty L / \mu$, with ρ_0 the fluid density, U_∞ the free stream velocity, L the flag length, and μ the dynamic viscosity.

The flag motion was governed by

$$\frac{\partial^2 \boldsymbol{X}}{\partial t^2} = \frac{\partial}{\partial s}\left(T \frac{\partial \boldsymbol{X}}{\partial s} \right) - \frac{\partial^2}{\partial s^2}\left(\gamma \frac{\partial^2 \boldsymbol{X}}{\partial s^2} \right) - \boldsymbol{F} \tag{3}$$

where s denotes the arc length, $\boldsymbol{X} = \boldsymbol{X}(s,t)$ the position, T the tension force, γ the bending rigidity and $\boldsymbol{F}$ the Lagrangian force exerted on the flexible flag by the fluid.

Equation (3) was non-dimensionalized by the flag density ρ_1, the flag length L, and the free stream velocity U_∞. It should be pointed out that the tension force can be determined from the inextensibility condition of flag (Huang *et al.* [16]), and the bending rigidity is defined as EI, with E the Young's modulus and I the second moment of area, which gives the non-dimensional value γ. The boundary conditions applied at the fixed end and the free end were

$$\boldsymbol{X} = \boldsymbol{X}_0,\ \frac{\partial^2 \boldsymbol{X}}{\partial s^2} = (0,0) \qquad \text{for the fixed end,} \tag{4}$$

$$T = 0,\ \frac{\partial^2 \boldsymbol{X}}{\partial s^2} = (0,0),\ \frac{\partial^3 \boldsymbol{X}}{\partial s^3} = (0,0) \qquad \text{for the free end.} \tag{5}$$

The interaction force between the flow and the structure was calculated using the feedback force by the relation

$$\boldsymbol{F} = \alpha \int_0^t (\boldsymbol{U}_{ib} - \boldsymbol{U})\, d\tau + \beta (\boldsymbol{U}_{ib} - \boldsymbol{U}), \tag{6}$$

where α and β are large negative free constants -10^5 and -10^3, respectively in Huang *et al.* (2007), $\boldsymbol{U}_{ib}$ is the fluid velocity obtained by interpolation at the immersed boundary, and $\boldsymbol{U}$ is the velocity of the flag expressed by $\boldsymbol{U} = d\boldsymbol{X}/dt$. On the other hand, $\boldsymbol{X}_{ib}$ and $\boldsymbol{U}_{ib}$ denote, respectively, the position and velocity of the immersed boundary, which were determined using the local Eulerian fluid velocity, as expressed by

$$\boldsymbol{U}_{ib}(s,t) = \int_\Omega \boldsymbol{u}(\boldsymbol{x},t)\,\delta(\boldsymbol{X}(s,t) - \boldsymbol{x})\, d\boldsymbol{x}, \tag{7}$$

where δ( ) denotes a smoothed approximation of the Dirac delta function, and Ω_f is the fluid region. Equation (8) provides an interpolation of the Eulerian fluid velocity at the Lagrangian points. In physics, equations (6) – (8) represent a stiff

spring system. This system connected the Lagrangian points on the immersed boundary to the surrounding fluid particles. After obtaining the Lagrangian force $\boldsymbol{F}$, the expression was transformed to the Eulerian form using the smoothed Dirac delta function,

$$\boldsymbol{f}(\boldsymbol{x},t)=\frac{\rho_1}{\rho_0 L_r}\int_\Gamma \boldsymbol{F}(s,t)\delta(\boldsymbol{x}-\boldsymbol{X}(s,t))ds\,. \tag{8}$$

where $\rho=\rho_1\big/\left(\rho_0 L\right)$, based on the non-dimensionalization steps, and Ω_s denotes the structure region. After discretization, the force was applied over a width of several grids, which supported the smoothed delta function.

The overall computational process, in which the present numerical algorithm was used to simulate the fluid–flexible body interactions, is summarized as follows:

(1) Initialize the computation parameters, the meshes, and the fluid and solid motions; set $\boldsymbol{X}_{ib}^0=\boldsymbol{X}^0$.

(2) At the nth time step, the fluid velocity $\boldsymbol{u}^n$ and the solid position $\boldsymbol{X}^n$ and velocity $\boldsymbol{U}^n$ are known. Interpolate the fluid velocity at the Lagrangian points to obtain $\boldsymbol{U}_{ib}^n$, and calculate the positions of the immersed boundary points $\boldsymbol{X}_{ib}^n$. Then calculate the Lagrangian momentum force $\boldsymbol{F}^n$.

(3) Map the Lagrangian momentum force onto the Eulerian grid. Obtain the updated fluid velocity field and pressure field.

(4) Substitute $\boldsymbol{F}^n$ into the flag motion equation and obtain the flag position at the new time step $\boldsymbol{X}^{n+1}$, as well as the velocity $\boldsymbol{U}^{n+1}=(\boldsymbol{X}^{n+1}-\boldsymbol{X}^n)/\Delta t$. Return to step 2 and march to the next time step.

The computational domain for the fluid flow ranged from -2 to 6 in the stream-

wise (x) direction and from -4 to 4 in the span-wise (y) direction, both of which directions were normalized by the flag length. The Eulerian grid size for the fluid was 512×350 in the stream-wise and span-wise directions, respectively, and the Lagrangian grid size for each flag was 64. The Eulerian grid was uniformly distributed along the x direction, and it was uniform in the y direction for $-2 \leq y \leq 2$, but stretched otherwise. The far-flow field was applied at the top and bottom boundaries as well as the inlet of the fluid domain, whereas the convective boundary condition was used at the outlet. The computational time step was set to 0.0002, which resulted in a CFL number of 0.1. The validation of the flow solver employing the immersed boundary method, as well as the structure solver for the flag motion, has been provided in Huang *et al [16]*.

Experimental Setup

Experiments were conducted in an open loop suction type wind tunnel composed of single fan as shown in figure 2. The wind tunnel had a cross-section of 1ft × 1ft and was capable of producing free-stream velocity U between 1 ms^{-1} to 15 ms^{-1}.

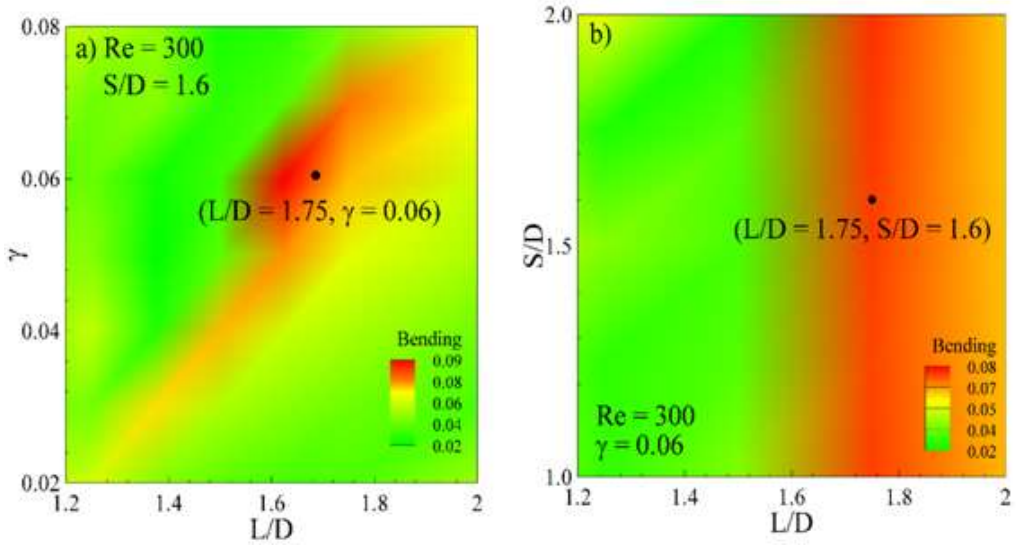

Figure 2: Contours of the bending energy for different a) L/D and γ, b) L/D and S/D

The leading edge of piezo flag was clamped with vertical rod of 2 mm dia. while trailing edge is free. Piezoelectric flag of measurement specialty having active length of 60mm, width of 12mm is used. Flag motion was observed using a slow-motion camera (Sony RX-100 IV) mounted at the top of the test section. 1000 images or frames were captured each second as the wind speed varied from $5ms^{-1}$ to $10ms^{-1}$. An oscilloscope (Gwinstek GDS-2062) is connected with piezoelectric flag to visualize and store wave form of voltage produce due to flag motion and to enhance the visualization of the flag motion; the test section was illuminated by two led lights (Mcopus TTV204). Overall setup was adjusted in wind tunnel test section in a way that it covers a maximum 10% of the frontal area. Behavior of flag motion and voltage produce ware recorded behind two cylinders of different diameters by varying velocity and distance to dia ratio i.e S/D.

MEASUREMENTS.

In experimental model, Piezo electric flag is placed behind Cylinder which act as bluff body. Piezo Flag is fixed from leading edge and free from trailing edge. Air blower is used to through streamline air at different velocity. Led lights are placed at the top of setup along with High Frame rate camera. Oscilloscope is connected to piezoelectric flag to measure voltage signal. Voltage of flag is measured, by varying velocity, S/D and L/D ratios. Meanwhile flag motion is also captured from top at High Frame Rate by varying same variables.

Chapter: 3

RESULTS & DISCUSSIONS.

Numerical results

A schematic diagram of the problem setup and the coordinate system for the downstream flag in the wake of the D-shaped half cylinder subjected to a uniform flow is plotted in figure 1. The computational configurations were set to be the same as described in the previous section. The initial position of the downstream flag was parallel with the stream-wise direction with its leading edge located at a stream-wise distance of 'S' from the origin. The downstream flag was inclined at an angle of 0.1π relative to the stream-wise direction. Even if the inclination angle was changed to -0.1π, the results obtained after several transient flapping periods remained unchanged. The flow patterns were investigated by conducting simulations over a long time period between 100 and 200 flapping periods. The flow patterns obtained after a minimum of 20 flapping periods were analyzed. The flow patterns and interaction forces were characterized in terms of the energy generated from the bending motion of the flag (Eb). The total potential energy is given by Zhu [17],

$$E = E_S + E_B, \tag{9}$$

where E_S and E_B are the stretching energy and the bending energy, respectively.

$$E_S = \frac{1}{2} K_S \int \left(\sqrt{\frac{\partial X}{\partial X_{ib}} \frac{\partial X}{\partial X_{ib}}} - 1 \right)^2 dX_{ib}, \tag{10}$$

$$E_B = \frac{1}{2} K_B \int \frac{\partial^2 X}{\partial X_{ib}^{\,2}} \frac{\partial^2 X}{\partial X_{ib}^{\,2}} dX_{ib}, \tag{11}$$

where K_S and K_B are the stretching coefficient and bending coefficient of the flag respectively. A quantitative characterization of the interaction behavior was supplemented by qualitative evaluations of the flag deformations and the vorticity contours within the flow, which provided an intuitive understanding of the vortex–flexible body interactions. Three parameters were chosen for optimization within the following ranges: the streamwise gap distance between the D-shaped half cylinder and the downstream flag ($1 \leq S/D \leq 2$), the bending coefficient of the flag ($0.02 \leq \gamma \leq 0.08$) and the length of the flag ($1.2 \leq L/D \leq 2.0$).The bending energy E_b of the downstream flag as a function of the length and the bending coefficient of the flag is plotted in figure 2a.

In this simulation, Re = 300 and $\rho=1$, these values remained unchanged unless otherwise stated. For a fixed streamwise gap distance of S/D = 1.6 (figure 2a), the bending energy contours clearly marks two regions, one representing the maximum bending energy in the range of $1.5 \leq L/D \leq 1.9$ for $0.04 \leq \gamma \leq 0.075$, and the second region representing the low bending energy is constituted by all the remaining L/D and γ values. The bending energy in the high bending region is four times larger than the low bending energy region. The details of the variation in the bending energy with the change in the length and the bending rigidity can be unfolded by analyzing the evolution of the tail position and the flag deformation shapes (figure 3), the power spectrum (figure 4) and the vorticity diagram (figure 5). Four points corresponding to the low and high bending energy are shown for different L/D ratio and γ.

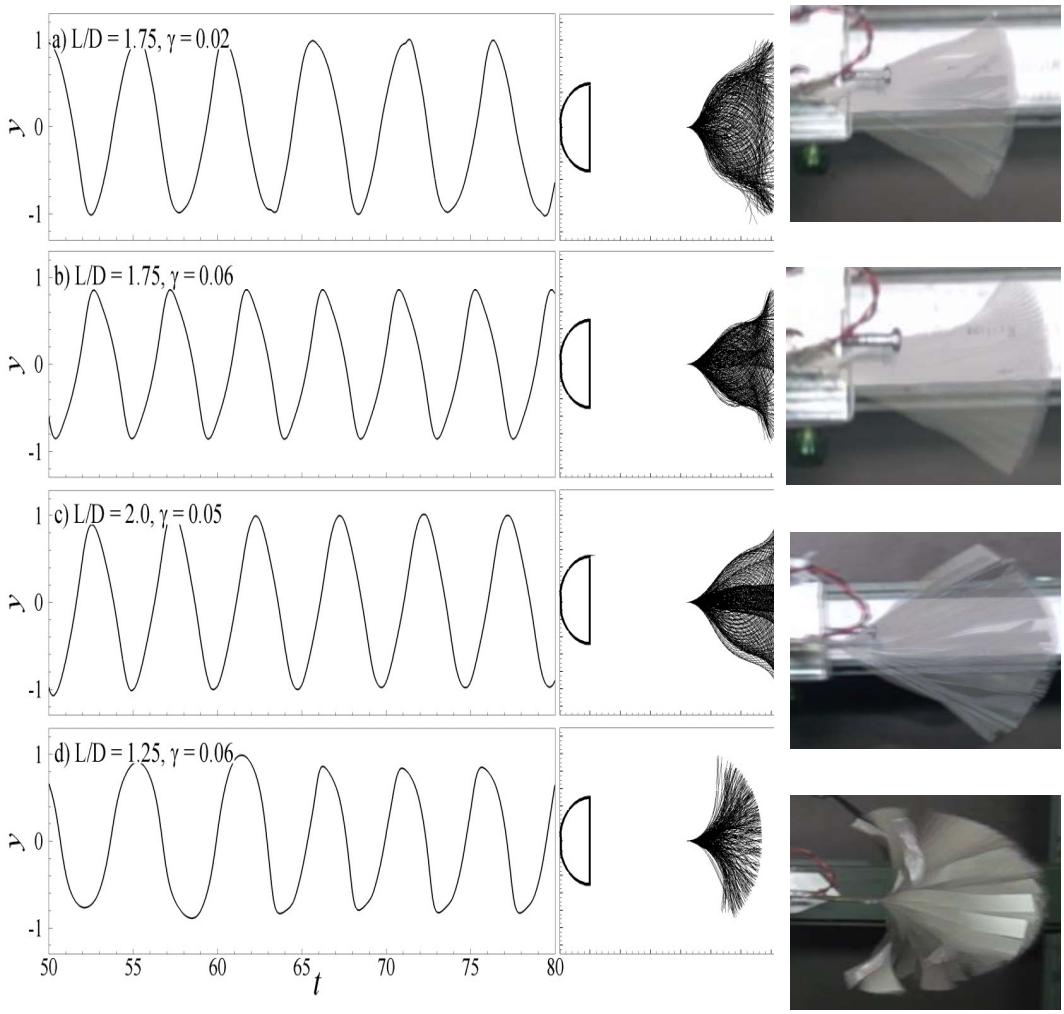

Figure 3: Evolutions of the tail position and corresponding flag deformations for different L/D and γ.

Figure 3 (a and b) shows the tail position evolution and flag deformation shapes with increase in the bending rigidity from 0.020 to 0.060 for the same L/D ratio, the tail position evolution shows the increase in the flapping frequency (seven peaks in 30 seconds as compared to six peaks) with the increase in the bending rigidity as well as

it is accompanied by the change in the flag deformation shape, the flag deformation shape remains constrained at increased bending coefficient (figure 3b) as compared to the low bending coefficient (figure 3a) by the virtue of the more stiffened flag.

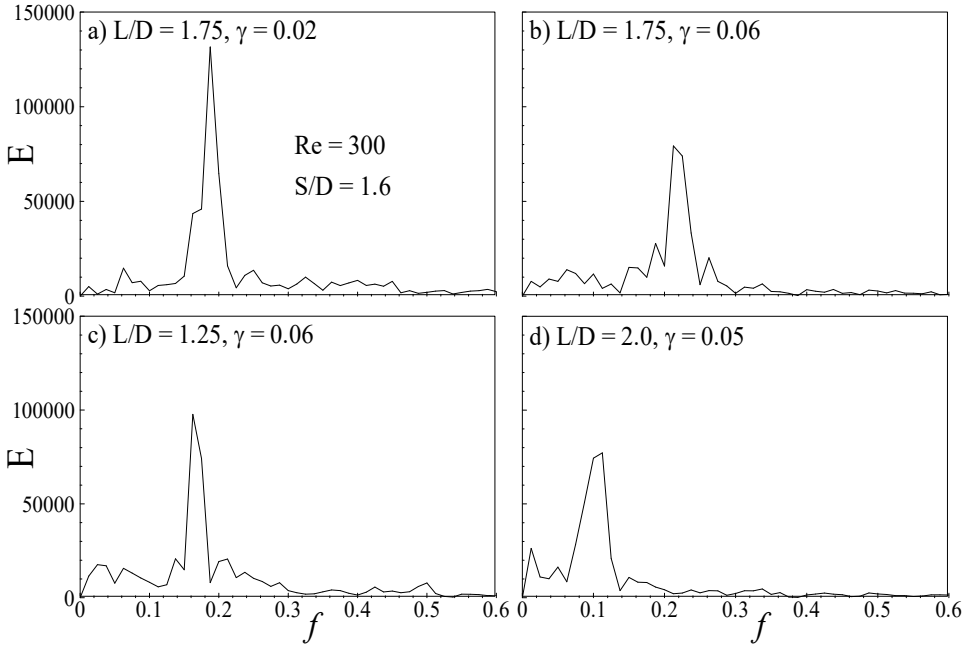

Figure 4: Power spectra for different L/D and γ.

The power spectrum of the corresponding two cases are shown in figure 4 (a and b). With the increase in the stiffness of the flag, the dominant frequency of the flag is increased from 0.19 to 0.22. For the less flexible flag in figure 3, 4 (a), the flag get significant deformation by the influence of the upstream vortices, this changes the flag shape significantly, resulting in decreasing the dominant frequency. The increase in the stiffness in figure 3, 4(a) causes more resistance to the upstream vortices, which decreases the effect of the upstream vortices resulting in the low deformation of the flag as well as increase in the dominant frequency which is near the natural frequency of the flag in a uniform flow. The length of the flag is increased to L/D=2.0 and the bending stiffness $\gamma = 0.05$, the bending energy is low while the flag deformation is significant (figure 3c) and the flapping frequency is lower than the high bending

emery region , as the L/D is decreased to 1.25 and the bending rigidity is increased to 0.06, the increased stiffness and the length has combined effect in the form of unidirectional curvature bending (figure 3d) and the flapping frequency is similar to low bending energy region. The power spectrum of these two low bending region points shows the dominant frequency is lower than the high bending energy case, the dominant frequency for L/D=2.0 and the bending stiffness $\gamma = 0.05$ is 0.1 (figure 4d) and with the decrease in the length, increase in bending rigidity for for L/D=1.25 and the bending stiffness $\gamma = 0.06$, the deformation switches from bi-curvature bending to the unidirectional curvature bending is also accompanied by the higher dominant frequency of 0.175 (figure 4c).

The vorticity contours are shown in figure 5, the flag is in the shear layer sheded by the D-shaped half cylinder for the length ratio above L/D=1.5, for the length below 1.5, the flag effects the upstream vortices by increasing the shear resistance to the upstream vortices which delays/blocks the upstream vortices and causes the two vortices to combine and create a shear layer for the downstream flag, while for the flag with reduced length and at the same streamwise gap distance, the vortices are completely sheded from the D-cylinder in the upstream sheded vortices interacts with the flag in the constructive manner where the positive vortices on the downside of the D-shared half cylinder interacts with the downside (positive vortices) of the flag and similarly negative vortices shed from the upper side of the D-cylinder interacts with the upper side (negative vortices) of the flag.

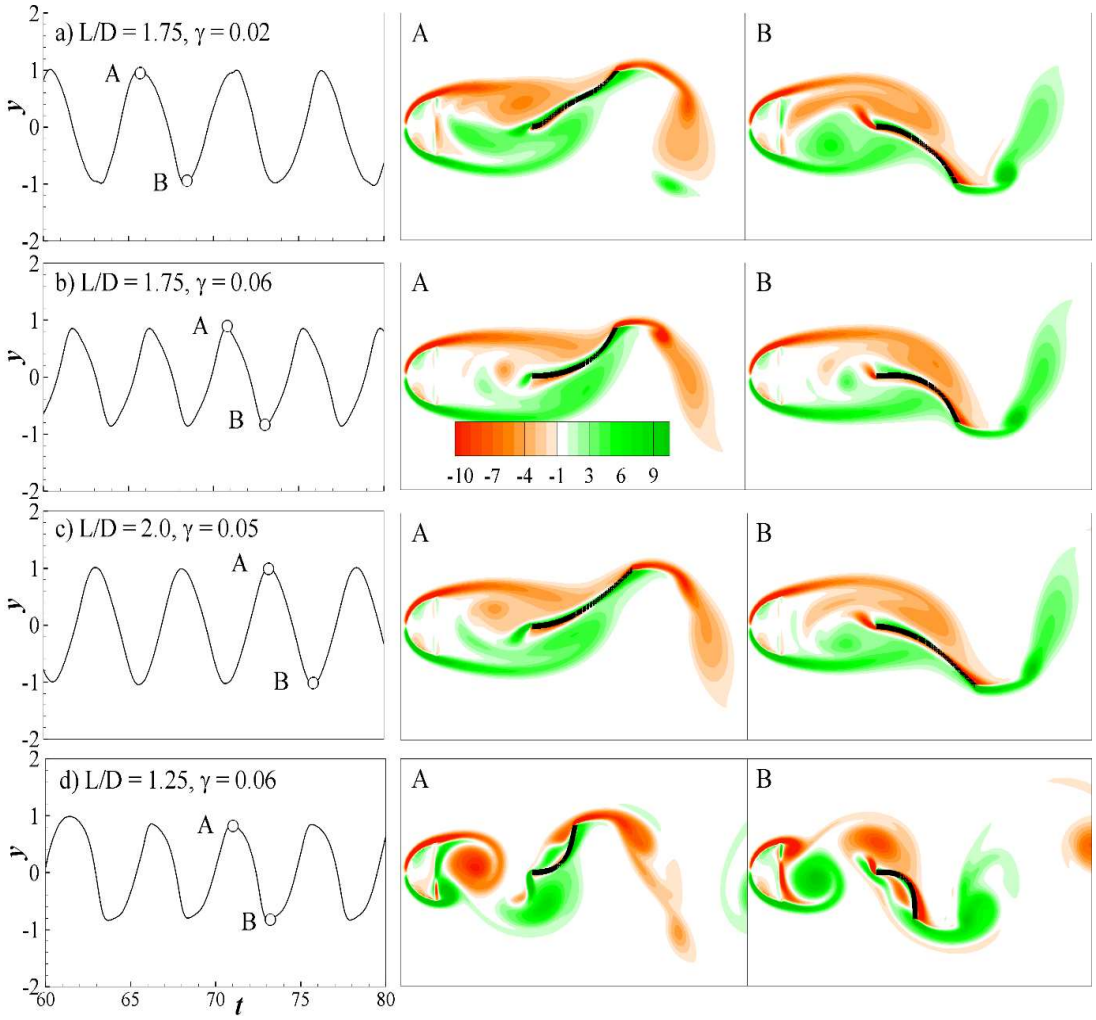

Figure 5: Contours of vorticity for different L/D and γ.

This effect is same for all the cases as the constructive mode, the constructive mode is dependent of the gap distance (Kim et. al. 2010). The creation of the shear layer causes suction zone in-front of the downstream flag, Beal et. al. (2006) reported the suction zone for the S/D<2.0, and this study reveals that it is also dependent on the L/D ratio by the action of increased shear resistance. The suction region creates the extra force on the flag which is higher for the L/D=1.75 and γ=0.06 shown by the absence of the vorticies in-front of the flag while for the other cases (figure 5a, c) the presence of vortices in-front of the flag causes lower effect of the suction zone resulting in the low bending energy. The map between the length to the bending

stiffness (figure 2a) gives the optimal L/D=1.75 and γ=0.06 for maximum energy harvesting.

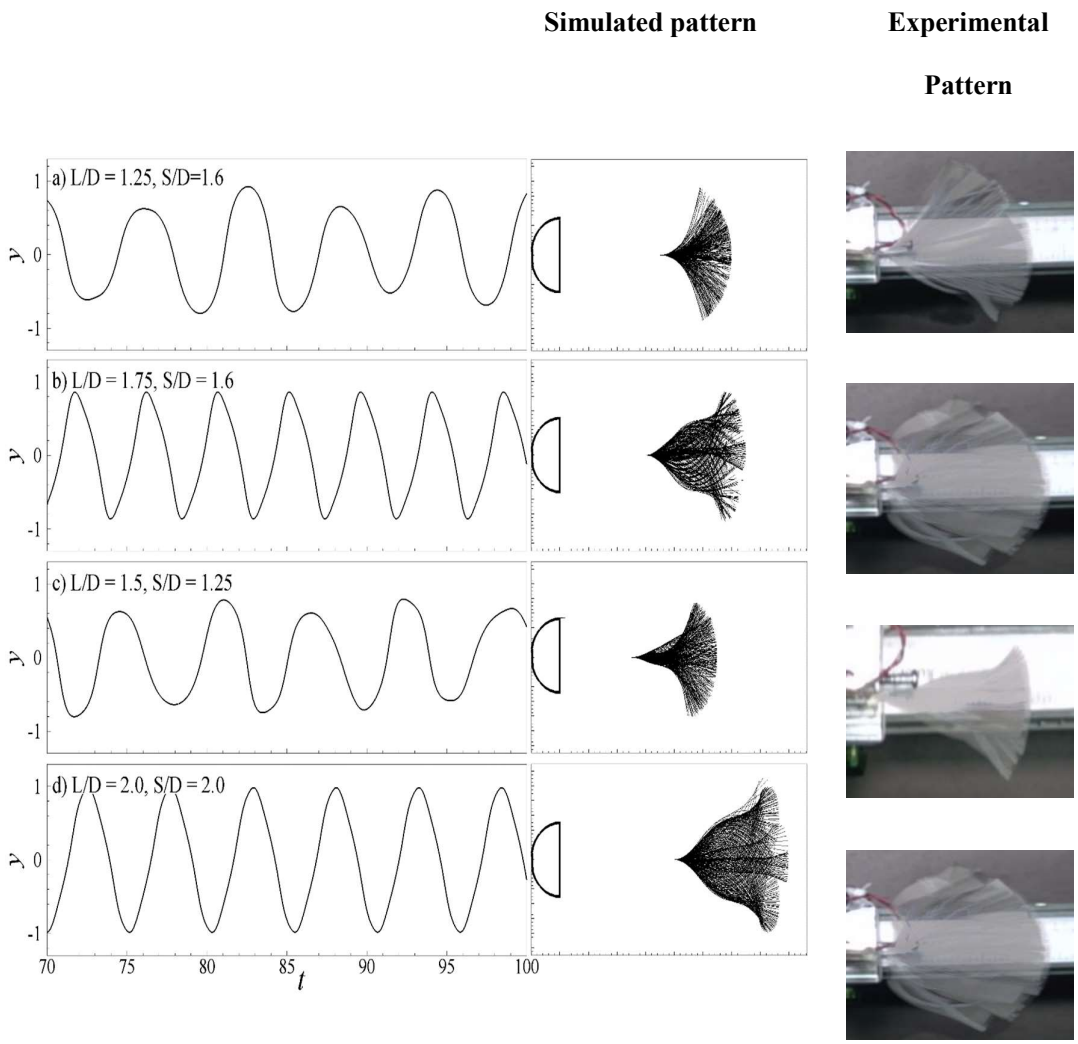

Figure 6: Evolutions of the tail position and corresponding flag deformations for different L/D and S/D.

The second map (figure 2b) showed the map between the length and the gap distance. Details are shown in the tail position evolution, the power spectrum and the vorticity flow field (figure 6, 7 and 8).

The tail position evolution shows the lowest energy region at L/D=1.25; S/D=1.75

(figure 7a) which corresponds to the lowest dominant frequency (f=0.15), as the energy is increased at L/D=1.5; S/D=1.25 (figure 7c), it is accompanied by the slight increase in the dominant frequency to f=0.18. The energy is increased at L/D=2.0; S/D=2.0 (figure 7d), it is accompanied by the slight increase in the dominant frequency to f=0.20. For the highest energy point at L/D=1.75; S/D=1.75 (figure 7b), it has the highest dominant frequency of f=0.22. The tail position evolution shows the two interesting finding, one is the frequency of the tail on the left side of figure 8, it is complementing the power spectrum (figure 7).

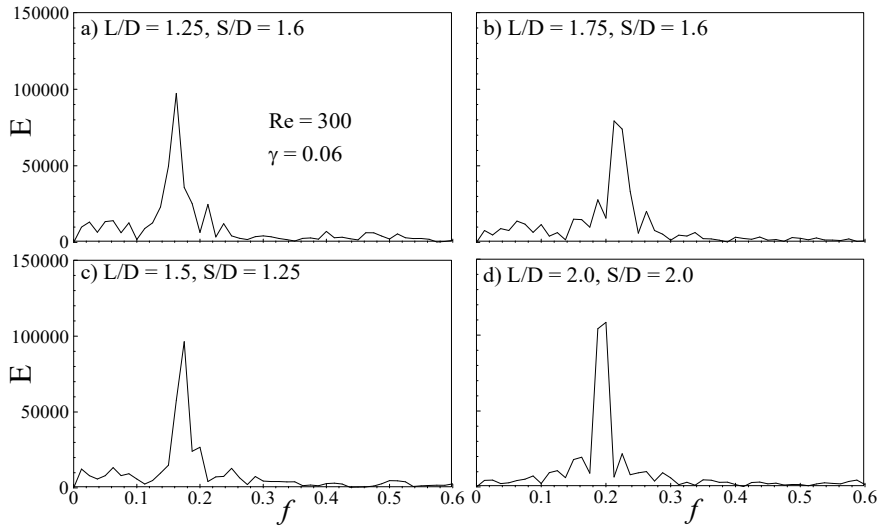

Figure 7: Power spectra for different L/D and S/D.

At the optimal location (figure 8b), there are seven peaks in the 30 seconds, while for the other low energy cases there are six peaks in 30 seconds. The other observation is the flag deformation shape, for the length ratio of the flag below L/D=1.75, unidirectional curvature deformation of the flag is observed (figure 8a, c), while the length above the L/D=1.75, there is bidirectional curvature deformation (figure 8b, d). The unidirectional/constrained deformation is attributed to the low bending energy. The bending rigidity and the gap distance is same but length is different causes jump

from the unidirectional to the bidirectional curvature deformation (figure 8a, b) which shows that the curvature change is function of the length of the flag. At the same bending rigidity, the shorter flag length causes constrained motion, as the shorter flag length results in the less effective area for exertion of the viscous forces by the fluid, while as the length is increased to L/D=1.75 provides the sufficient surface area of the flag to exert more viscous forces on the flag to cause the bidirectional curvature flapping. The vorticity flow field (figure 8) shows the sheded vorticies interaction with the flag for L/D=1.25 and S/D=1.6 (figure 8a) while for the other length and stream wise distances there is a shear layer and suction zone (figure(8b, c and d).

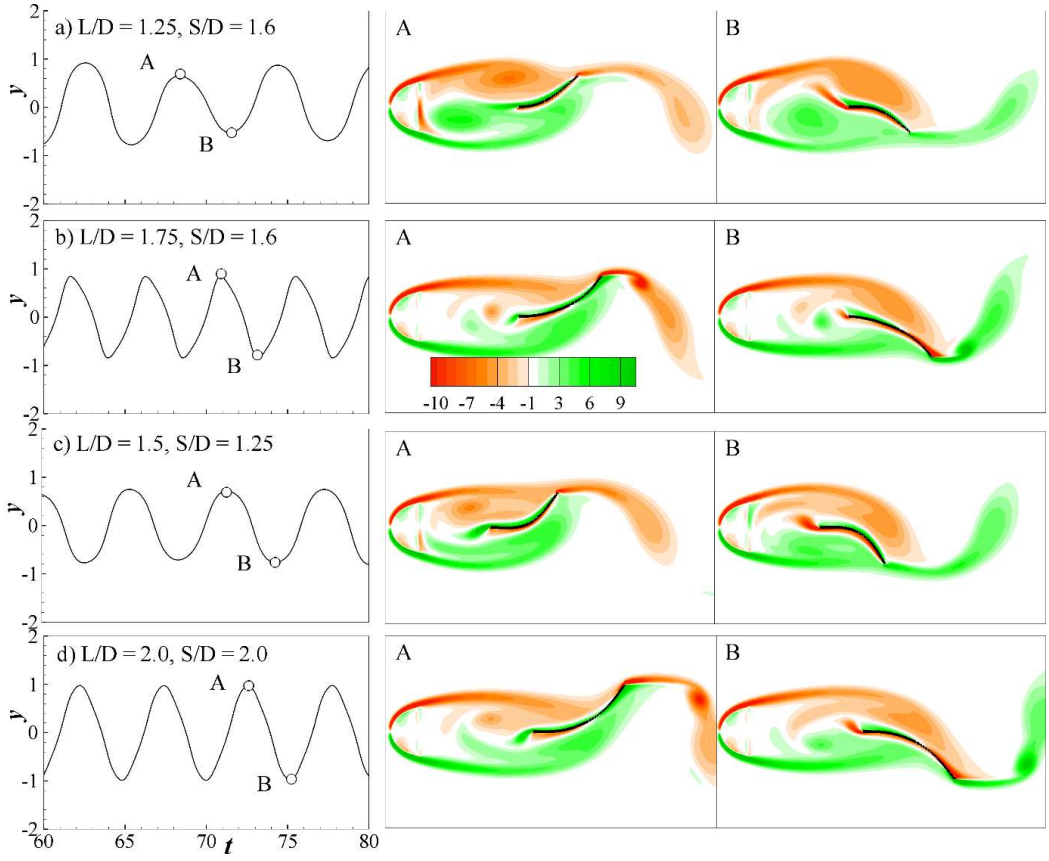

Figure 8: Contours of vorticity for different L/D and S/D.

No vortices in-front of the high bending energy zone (figure 8b) as compared with the vortices in the suction zone shows the effect of the suction zone on the bending

energy. This map (figure 2b) gives the optimal length and the gap distance for maximum energy harvesting (L/D=1.75, S/D=1.75) while optimal bending rigidity is γ=0.06.

Chapter: 4

CONCLUSIONS.

In experimentation, because of physical constraints and Wind tunnel limitations parameters as used in simulation cannot be achieved. Experimentation is done at by varying Re values from 25000 to 30000 , S/D from 1 to 5 and L/D from 1 to 2. For a fixed L/D=1 (figure 9a), the voltage contours clearly mark two regions, one representing the maximum voltage in the range of $3.0 \leq S/D \leq 5$ for $25000 \leq Re \leq 30000$, and the second region representing the low voltage is constituted by all the remaining S/D and Re values. The Voltage produces in the high voltage region is 21%more than the low voltage region.

In 2nd graph for L/D = 2 a similar behavior was observed. i.e maximum voltage production region was formed at $S/D \geq 3.0$ and $25000 \leq Re \geq 35000$ while low voltage region was formed at all the remaining S/D and Re values.

While increasing L/D ration from 1 to 2 it was observed that high voltage region begins to expand. At L/D = 1 high region more concentrated toward Re = 25000 while at L/D = 2 it moves toward Re=30000 and spread till Re=35000. Lower zone Value at L/D =1 is 0.20V while at L/D = 2 lower zone value increases to 0.225V which shows more power production by increasing L/D ratio.

We examined the dynamics of energy harvesting flexible flag behind a half cylinder undergoing passive flapping mode subjected to a uniform viscous flow by using the immersed boundary method. The analysis was carried out under different conditions by varying S/D, L/D and γ. For the passive flapping, the increase in bending stiffness for $0.04 \leq \gamma \leq 0.08$ and the length ratio of the flag ($1.5 \leq L/D \leq 1.9$)

causes increase in the bending energy. The increase in the bending stiffness is accompanied by the increase in the flag deformation as well as the dominant and the flapping frequency is increased. Constructive mode is observed for the optimal bending energy region when the stream wise distance is increased. Also, the unidirectional curvature is attributed to the low bending energy while the bidirectional curvature is attributed to the high bending energy case. The downstream flag was synchronized by the vortices shed from the upstream D cylinder. The frequency of the tail flapping is same for both case but the amplitude of the tail flapping is different, the amplitude is higher for the high bending energy case and vice versa. The tail vortices corresponding to the high bending energy case has higher energy than the low bending energy case, this depicted the energy harvesting from the upcoming vortices by intercepting while low energy can be harvested if the flag passes between the upstream vortices. Similar vortex interception and slaloming mode are observed with the variation of the pitching and the heaving amplitudes. By analyzing the passive flapping we obtained the optimal length of the flag, gap distance between the flag and D cylinder and bending rigidity. Experimentation clearly depicts that by increasing stream wise distance between cylinder and flag higher values of voltage is obtained i.e electrical energy and similar relation was observed L/D ratio. It was also observed that more power was obtained at higher values of L/D ratio. Higher value of Electrical energy is obtained at $L/D = 2$, $Re = 30000$ and $S/D \geq 3.0$.

Energy harvesting from air by using piezo electric material is very new and interesting concept particularly when there is a great demand of renewable energy with 0% carbon emission and environmental friendly. It is an optimum solution for low energy consumption devices like sensors and small devices. Piezo electric Converts mechanical vibration energy into electric energy. This energy can be stored

in batteries like lithium polymer, Nimh for later usage. It is very good because of its reliability and portability as it uses free stream air without any complex circuit and weight.

REFERENCES.

[1] C. Lins *et al.*, "Renewables 2014 global status report," ed, 2014.

[2] J. Allen and A. Smits, "Energy harvesting eel," *Journal of fluids and structures,* vol. 15, no. 3-4, pp. 629-640, 2001.

[3] A. Barrero-Gil, G. Alonso, and A. Sanz-Andres, "Energy harvesting from transverse galloping," *Journal of Sound and Vibration,* vol. 329, no. 14, pp. 2873-2883, 2010.

[4] M. M. Bernitsas, K. Raghavan, Y. Ben-Simon, and E. Garcia, "VIVACE (Vortex Induced Vibration Aquatic Clean Energy): A new concept in generation of clean and renewable energy from fluid flow," *Journal of offshore mechanics and Arctic engineering,* vol. 130, no. 4, p. 041101, 2008.

[5] Z. Peng and Q. Zhu, "Energy harvesting through flow-induced oscillations of a foil," *Physics of fluids,* vol. 21, no. 12, p. 123602, 2009.

[6] K. Singh, S. Michelin, and E. De Langre, "The effect of non-uniform damping on flutter in axial flow and energy-harvesting strategies," in *Proc. R. Soc. A*, 2012, p. rspa20120145: The Royal Society.

[7] M. S. Triantafyllou, A. H. Techet, and F. S. Hover, "Review of experimental work in biomimetic foils," *IEEE Journal of Oceanic Engineering,* vol. 29, no. 3, pp. 585-594, 2004.

[8] Q. Zhu, M. Wolfgang, D. Yue, and M. Triantafyllou, "Three-dimensional flow structures and vorticity control in fish-like swimming," *Journal of Fluid Mechanics,* vol. 468, pp. 1-28, 2002.

[9] J. C. Liao, D. N. Beal, G. V. Lauder, and M. S. Triantafyllou, "Fish exploiting vortices decrease muscle activity," *Science,* vol. 302, no. 5650, pp. 1566-1569, 2003.

[10] W. McKinney and J. DeLaurier, "The wingmill: an oscillating-wing windmill," *Journal of energy,* vol. 5, no. 2, pp. 109-115, 1981.

[11] T. Y. Wu and A. T. Chwang, "Extraction of flow energy by fish and birds in a wavy stream," in *Swimming and flying in nature*: Springer, 1975, pp. 687-702.

[12] J. Grue, A. Mo, and E. Palm, "Propulsion of a foil moving in water waves," *Journal of fluid mechanics,* vol. 186, pp. 393-417, 1988.

[13] T. Wu, "Extraction of flow energy by a wing oscillating in waves," 1971.

[14] H. Isshiki and M. Murakami, "A theory of wave devouring propulsion (4th report)," *Journal of the society of naval architects of Japan,* vol. 1984, no. 156, pp. 102-114, 1984.

[15] J. D. Eldredge, "Dynamically coupled fluid–body interactions in vorticity-based numerical simulations," *Journal of Computational Physics,* vol. 227, no. 21, pp. 9170-9194, 2008.

[16] W.-X. Huang, S. J. Shin, and H. J. Sung, "Simulation of flexible filaments in a uniform flow by the immersed boundary method," *Journal of Computational Physics,* vol. 226, no. 2, pp. 2206-2228, 2007.

[17] L. Zhu, "Interaction of two tandem deformable bodies in a viscous incompressible flow," *Journal of Fluid Mechanics,* vol. 635, pp. 455-475, 2009.